frontiers | Frontiers in Chemistry

TYPE Review
PUBLISHED 22 December 2022
DOI 10.3389/fchem.2022.1098209

OPEN ACCESS

EDITED BY
Guigao Liu,
Nanjing University of Science and Technology, China

REVIEWED BY
Ning Zhang,
Central South University, China
Haiying Jiang,
Northwest University, China
Shengyao Wang,
Huazhong Agricultural University, China

*CORRESPONDENCE
Xianguang Meng,
mengxg_materchem@163.com
Xiaole Xian,
xianxiaole520@126.com
Jingjing Zhao,
zhaojingjing@ncst.edu.cn

SPECIALTY SECTION
This article was submitted to Catalytic Reactions and Chemistry, a section of the journal Frontiers in Chemistry

RECEIVED 14 November 2022
ACCEPTED 12 December 2022
PUBLISHED 22 December 2022

CITATION
Wen H, Huang S, Meng X, Xian X, Zhao J and Roy VAL (2022), Recent progress in the design of photocatalytic H_2O_2 synthesis system.
Front. Chem. 10:1098209.
doi: 10.3389/fchem.2022.1098209

Recent progress in the design of photocatalytic H_2O_2 synthesis system

Haobing Wen[1], Sen Huang[1], Xianguang Meng[1]*, Xiaole Xian[2]*, Jingjing Zhao[3]* and Vellaisamy A. L. Roy[4]

[1]Hebei Provincial Laboratory of Inorganic Nonmetallic Materials, College of Materials Science and Engineering, North China University of Science and Technology, Tangshan, China, [2]Traditional Chinese Medical College, North China University of Science and Technology, Tangshan, China, [3]School of Pharmacy, North China University of Science and Technology, Tangshan, China, [4]James Watt School of Engineering, University of Glasgow, Glasgow, United Kingdom

Photocatalytic synthesis of hydrogen peroxide under mild reaction conditions is a promising technology. This article will review the recent research progress in the design of photocatalytic H_2O_2 synthesis systems. A comprehensive discussion of the strategies that could solve two essential issues related to H_2O_2 synthesis. That is, how to improve the reaction kinetics of H_2O_2 formation *via* $2e^-$ oxygen reduction reaction and inhibit the H_2O_2 decomposition through a variety of surface functionalization methods. The photocatalyst design and the reaction mechanism will be especially stressed in this work which will be concluded with an outlook to show the possible ways for synthesizing high-concentration H_2O_2 solution in the future.

KEYWORDS

photocatalysis, oxygen reduction reaction, H_2O_2 synthesis, cocatalyst, surface modification, ion doping

1 Introduction

H_2O_2 is an indispensable chemical in daily life. It has many applications in fields such as biology (Chang et al., 2021; Noh et al., 2020; Guarino et al., 2019), medicine (Andersen et al., 2006; Kozlova et al., 2015; Wang Y. et al., 2020), chemical industry (Chung et al., 2020; Zhang et al., 2021), environmental protection (Dinakar et al., 2020; Moreno, 2011). As a clean oxidant, the decomposition of H_2O_2 only yields H_2O, which does not pose an environmental risk. Currently, the anthraquinone (AQ) method is the main method for the industrial production of H_2O_2 (Sterenchuk et al., 2018). The AQ method for H_2O_2 synthesis includes two steps: hydrogenation and oxidation (Campos-Martin et al., 2006; Halder and Lawal, 2007; Gao et al., 2020). In this method, AQ is used as an intermediate, and the hydrogenation reaction is first performed with palladium catalyst (Chen, 2008; Edwards and Hutchings, 2008; Han et al., 2015). Then, oxygen is added to oxidize the hydroanthraquinone (AQH_2) back to AQ and produce H_2O_2 (Figure 1). However, the AQ method not only has the risk of explosion, but consumes a lot of energy and organic solvent (Chen, 2008; Jia et al., 2018). Therefore, it is crucial to develop a safe and direct method to synthesize H_2O_2. The methods of direct H_2O_2 synthesis mainly includes electrocatalysis (Apaydin et al., 2018; Du et al., 2020; Sun et al., 2020;

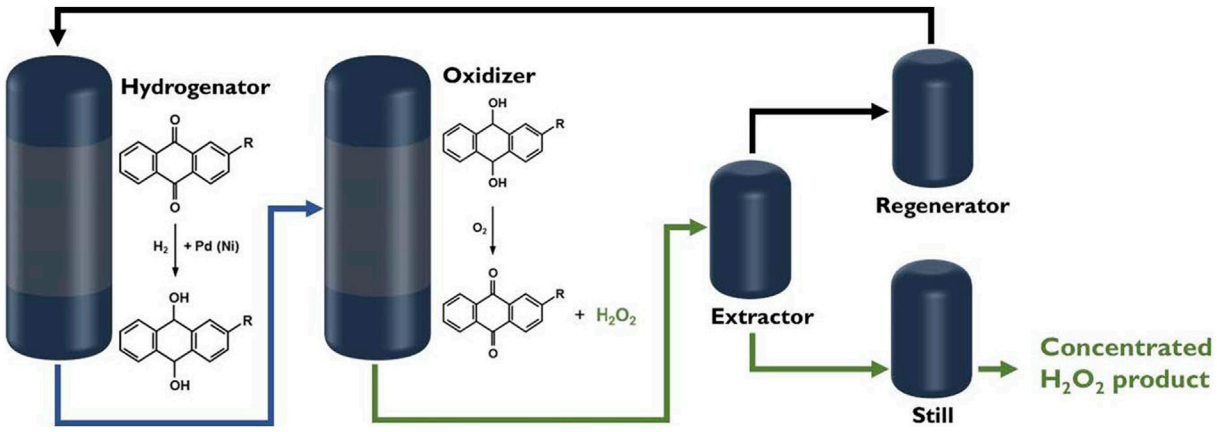

FIGURE 1
Flow chart of synthesis of H_2O_2 by AQ method (Yang et al., 2018).

Shu et al., 2021), photocatalysis (Chen et al., 2018; Kormann et al.), and thermal catalysis (Adams et al., 2021). The electrocatalytic H_2O_2 synthesis has a high yield but it needs to consume useful electricity. Thermocatalytic H_2O_2 synthesis from oxygen and hydrogen also faces the risk of explosion when mixing the gases. The emerging photocatalytic H_2O_2 synthesis only uses solar energy to drive reaction without introducing hydrogen.

During photocatalytic H_2O_2 synthesis, the electron is first excited from the valence band to the conduction band of the photocatalyst. Then, it participates in oxygen reduction reactions (ORR) on the surface to generate H_2O_2. H_2O_2 synthesis *via* oxygen reduction can undergo two pathways. The step-by-step single-electron pathway is the first one (Eqs. 1–3), which is characterized by the presence of superoxide (HO_2•) intermediate. The other is the direct two-electron ($2e^-$) pathway (Eq. 1 and Eq. 4). Which one of these occurs can be confirmed by detecting the intermediate HO_2• (Viswanathan et al., 2012; Baran et al., 2018; Fukuzumi et al., 2018; Haider et al., 2019; Anantharaj et al., 2021; Yang, 2021; Guo et al., 2022).

$$\mathbf{Photocatalyst + hv \rightarrow e^- + h^+} \quad (1)$$

$$\mathbf{O_2 + e^- + H^+ \rightarrow \bullet OOH} \quad (2)$$

$$\mathbf{\bullet OOH + e^- + H^+ \rightarrow H_2O_2} \quad (3)$$

$$\mathbf{O_2 + 2e^- + 2H^+ \rightarrow H_2O_2} \quad (4)$$

Photocatalytic H_2O_2 generation is also accompanied by a decomposition reaction, which is the root cause of poor reaction stability. The decomposition process includes photolysis and light-independent decomposition. Taking TiO_2 as an example, photolysis can occur mainly in four ways (I) photogenerated electrons reduce H_2O_2 to $OH^-$and •OH; (II) photogenerated holes oxidize hydrogen peroxide to O_2 or superoxide radical $\bullet O_2^-$; (III) The titanium peroxide complex (Ti-OOH) formed on the surface by the interaction of TiO_2 and H_2O_2 gradually degrades under visible light; (IV) direct decomposition of H_2O_2 under ultraviolet light. H_2O_2 can also be decomposed in ways independent of light, such as pH and temperature.

The formation and decomposition performance of hydrogen peroxide are closely related to the surface properties of semiconductor photocatalysts. First, the high selectivity of cocatalysts to $2e^-$ ORR is needed to improve the photocatalytic H_2O_2 formation. Second, the functional modifier on photocatalyst can inhibit the decomposition of H_2O_2. These strategies indicate that surface functionalization of photocatalysts is very important. Considering these issues, we review the recent advances in the design of photocatalysts for H_2O_2 synthesis in this work.

2 Effect of cocatalyst on photocatalytic activity

2.1 Noble metal cocatalysts

Precious metals are widely used as cocatalysts in electrocatalysis and photocatalysis, while they also show excellent performance in ORR (Zinola et al., 1995; Chen et al., 2017a; Cai et al., 2019; Ignaczak et al., 2019; Jeon et al., 2020). Pt has good ORR performance and strong binding ability to intermediates such as O_2 and OH•. When using Pt, generating H_2O *via* $4e^-$ORR is favored, but it has poor selectivity for $2e^-$ORR (Kim J. et al., 2018; Chen J. Y. et al., 2020). Among these noble metals, Au has the best selectivity for $2e^-$ ORR, which has achieved efficient photocatalytic H_2O_2 synthesis in photocatalytic reaction (Jirkovsky et al., 2010; Jirkovsky et al., 2011; Zuo et al., 2019a; Ignaczak et al., 2019; Sun et al., 2020). Zuo et al. studied the influence of a series of noble metal co-catalysts (Pd, Pt, Au, and Ag) on the performance of photocatalytic H_2O_2 synthesis over g-C_3N_4. They found that the maximum activity could be achieved when the Au loading amount is very low (0.01 wt%) on

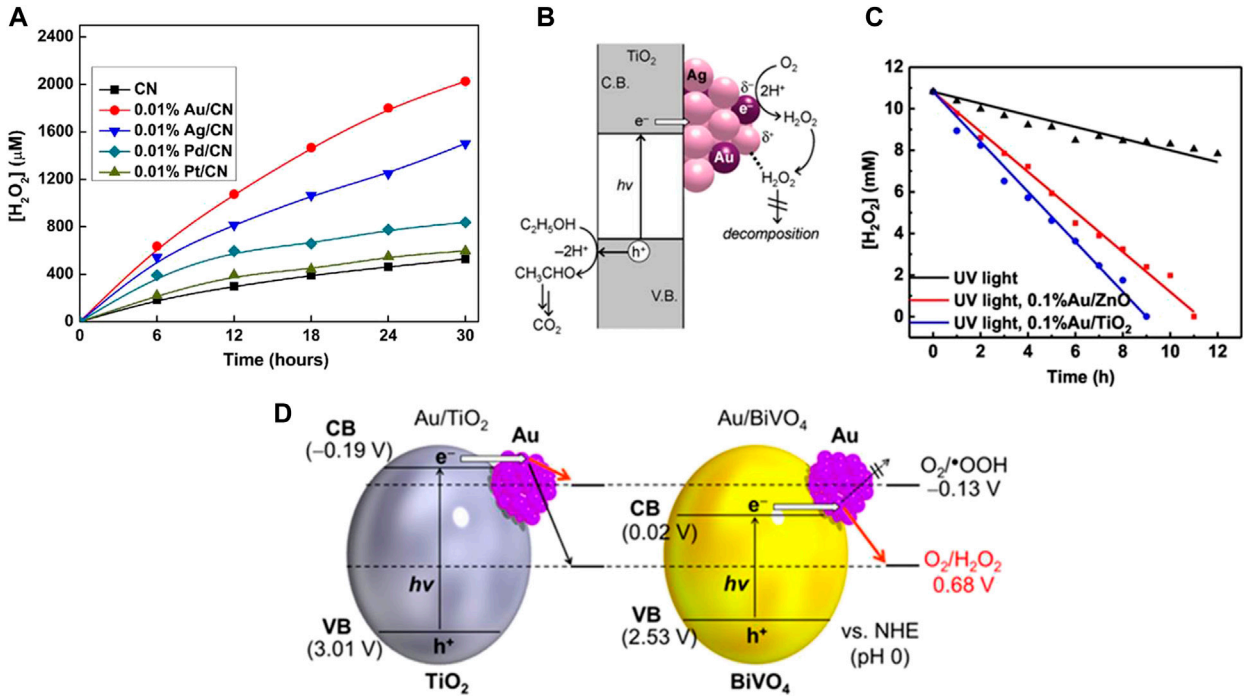

FIGURE 2
(A) Under visible light irradiation (λ > 420 nm), different noble metal loaded CN photocatalyzed H_2O_2 activity (Zuo et al., 2019a). **(B)** Mechanism for photocatalytic production of H_2O_2 on Au-Ag/TiO_2 catalyst (Tsukamoto et al., 2012). **(C)** Photodecomposition of H_2O_2 under UV light with and without photocatalysts (Meng et al., 2020); **(D)** Energy diagrams for Au/TiO_2 and Au/$BiVO_4$, and reduction potential of O_2 (Hirakawa et al., 2016).

g-C_3N_4 (Figure 2A) (Zuo et al., 2019a). A similar study showed that Au cocatalyst has the highest activity among different precious metals modified g-C_3N_4 samples (Kim H. I. et al., 2018). Similar high activity was observed over Au loaded TiO_2-based photocatalysts (Tsukamoto et al., 2012), (Li L. et al., 2021; Feng et al., 2021).

The H_2O_2 yield of Au-Ag alloy cocatalyst supported on the surface of TiO_2 was 2.3 times and 3.4 times higher than that of single Au or Ag cocatalyst. The reason was that the loaded Au-Ag alloy was conducive to the separation of electron holes, and the efficient photocatalytic reduction of O_2 on Au atom promotes the formation of H_2O_2 (Figure 2B) (Tsukamoto et al., 2012). However, the activity of Au deposition on ZnO was better than that on TiO_2, which is attributed to the more inert surface properties of ZnO than TiO_2 when decomposing H_2O_2 (Figure 2C) (Meng et al., 2020).

Hirakawa et al. (Hirakawa et al., 2016) suggested that activity of Au cocatalyst is affected by the band structure of semiconductor photocatalytsts. They employed Au/$BiVO_4$ photocatalyst to successfully produce H_2O_2 under visible light irradiation (λ> 420 nm). Since the conduction band potential of $BiVO_4$ (0.02 V vs SHE) is more positive than the one-electron ORR potential (-0.13V) and more negative than the $2e^-$ ORR (0.68 V vs SHE), the $2e^-$ ORR can be selectively promoted while the one-electron ORR is inhibited. Compared with TiO_2, $BiVO_4$ has a narrower band gap, which indicates that $BiVO_4$ has a better ability to utilize visible light and 2e ORR selectivity than TiO_2 (Figure 2D).

2.2 Non-precious metal cocatalysts

Considering the scarcity and high cost of precious metals, developing non-precious metal co-catalysts for $2e^-$ORR is crucial (Zhang J. et al., 2020; Yan et al., 2020). For example, the surface of g-C_3N_4 was loaded with AQ as a cocatalyst. Its activity reached 361 μm/h, which was 4.4 times that of pure g-C_3N_4 and comparable to some precious metals. This is because, in addition to the $2e^-$ ORR reaction catalyzed by pure g-C_3N_4, another H_2O_2 synthesis pathway *via* hydrogenation ($AQ + 2H^+ + 2e^- \rightarrow AQH_2$) and dehydrogenation ($AQH_2 + O_2 \rightarrow AQ + H_2O_2$) plays a key role in the photocatalytic reaction (Kim H. I. et al., 2018). For CoP loaded on g-C_3N_4, the catalytic activity of CoP/g-C_3N_4 (70 $\mu M \bullet h^{-1}$) was similar to that of Au/g-C_3N_4 (67.56 $\mu M \bullet h^{-1}$) (Zuo et al., 2019a). This can be attributed to the accelerated separation and transfer of g-C_3N_4 photogenerated charge by CoP (Peng et al., 2017). The method of loading quantum dots to improve visible light absorption and electron mobility is also beneficial to photocatalytic synthesis of H_2O_2

TABLE 1 Activities of photocatalysts with different types of cocatalyst.

Photocatalyst	Catalyst mass	Incident light	Cocatalyst content	Reaction condition	H_2O_2 activity	Reaction mechanism*	References
Ag@U-g-C_3N_4-NS-1.0	0.1 g (100 ml)	300 W Xe lamp (100 mW•cm^{-2})	Ag 1 wt%	pH = 3, O_2, 1 mol/L HClO	1.975 × 10^{-6} M•min^{-1}	—	Cai et al. (2019)
Au/C_3N_4-500(N_2)	1 g/L	300 W Xe lamp (λ > 420 nm)	Au 2 wt%	pH = 3, O_2, 5 vol % IPA	1320 μmol•L^{-1} (4 h)	—	Chang et al. (2018)
Au/Bi_2O_3-TiO_2	200 mg (200 ml)	300 W Xe lamp (λ > 420 nm)	Au 0.1 wt%, Bi: Ti = 1 wt%	O_2, 4 wt% C_2H_5OH	11 mM (12 h)	(II)	Feng et al. (2021)
Au/$BiVO_4$	50 mg (30 ml)	2 kW Xe lamp (λ > 420 nm)	Au 0.2 wt%	O_2, 10 vol% EtOH	40.2 μM (10 h)	(I)	Hirakawa et al. (2016)
Au/CN	400 mg (100 ml)	300 W Xe lamp (λ > 420 nm)	Au 0.01 wt%	pH = 8.5, O_2, 10 vol% C_2H_5OH	2027 μM (30 h)	(I)	Zuo et al. (2019a)
Au/β-CD-CN	0.4 g (100 ml)	2 kW Xe lamp (λ > 420 nm)	Au 0.05 wt%	O_2, 10 vol% C_2H_5OH	3000 μM (30 h)	(I)	Zuo et al. (2020)
Ag/β-CD-CN	0.4 g (100 ml)	300 W Xe lamp (λ > 420 nm)	Ag 0.05 wt%	O_2, 10 vol% C_2H_5OH	1000 μM(30 h)	(I)	Zuo et al. (2020)
Au/ZnO	0.2 g (200 ml)	300 W Xe lamp (UV-REF)	Au 0.1 wt%	O_2, 4 wt% C_2H_5OH, 0.1M NaF	1.5 $mmol^{-1}$•h^{-1}	Au>0.1wt% (I) Au<0.1wt% (II)	Meng et al. (2020)
Au/SnO_2-NR#TiO_2	10 mg (10 ml)	300 W Xe lamp (λ > 430 nm)	—	O_2, 4% EtOH	60 μM (6 h)	(I)	Awa et al. (2020)
Au-Ag/TiO_2	5 mg (5 ml)	450 W high pressure Hg lamp (λ > 280 nm)	Au 0.1 mol%, Ag 0.4 mol%	O_2, 4 vol% C_2H_5OH	3.4 m′M (12 h)	(I)	Tsukamoto et al. (2012)
Au@MoS_2	0.05 g (50 ml)	300 W Xe lamp	Au 0.5 wt%	pH = 9, O_2	1100 μM (12 h)	(I) (III)	Song et al. (2019)
Pt/TiO_2	1 mg (20 ml)	500 W Hg lamp (λ > 300 nm)	Pt 1 wt%	Ar	5096 μmol•L^{-1}•h^{-1}	$2H_2O \rightarrow H_2+H_2O_2$	Wang et al. (2019b)
Au-(ZT)-Al	5 cm × 5 cm	400–650 nm	17 wt%	pH = 7, 5 vol% C_2H_5OH	0.099 μM/min	—	Willis et al. (2020)
Pt-KCN(5)	0.2 g (200 ml)	400–800 nm	Pt 1 wt%	Remove air	620 μmol•g^{-1}	(II)	Hu et al. (2020)
Au/F-TiO_2	0.2 g (200 ml)	300 W Xe lamp (λ > 420 nm)	Au 0.1wt%	O_2, 4 wt% C_2H_5OH	6.5 mM (12 h)	(II)	Li et al. (2021a)
Cu(hfacac)$_2$/ m-$BiVO_4$	80 mg (80 ml)	300 W Xe lamp (λ > 430 nm)	400 μM Cu(hfacac)	O_2, H_2O:ACN: EtOH = 86:10:4	120 μM (2 h)	(I)	Teranishi et al. (2020)
CoP/g-C_3N_4	20 mg (50 ml)	300 W Xe lamp (λ > 420 nm)	CoP 1.76 wt%	O_2, 10 vol% C_2H_5OH	140 μM (2 h)	(II)	Peng et al. (2017)
AQ/C_3N_4	0.5 g/L	100 mW•cm^{-2} 150 W Xe lamp	AQ 10 wt%	O_2, 10 vol% IPA	361 μmol•L^{-1}•h^{-1}	(II)	Kim et al. (2018b)
NiS@g-C_3N_4-30	10 mg (10 ml)	300 W Xe lamp (λ > 420 nm)	Ni 2.06 wt%	O_2, 10 vol% C_2H_5OH	400 μM (1 h)	(II)	Kim et al. (2018b)
Ti_3C_2/TiO_2	50 mg (30 ml)	9 W white lamp (λ = 365 nm)	10% Ti_3C_2	O_2, 10 vol% C_2H_5OH	359.43 μmol•h^{-1}	(II)	Chen et al. (2021)
SN-GQDs/TiO_2	25 mg (50 ml)	500 W Xe lamp (λ > 300 nm)	SN-GQDs 0.5 wt%	pH = 3, O_2, 6 vol % IPA	451 μM (60 min)	(II)	Zheng et al. (2018)
FeOOH QDs/CQDs/ g-C_3N_4	25 mg (100 ml)	300 W Xe lamp (λ > 420 nm)	FeOOH QDs 2 wt%	10 ml IPA	224.24 μmol h^{-1} •g	(II)	Zhang et al. (2020b)

*The reaction mechanism is direct two electron oxygen reduction reaction, The reaction formula is: $O_2 + 2e^- + 2H^+ \rightarrow H_2O_2$ (I); Step by step one electron oxygen reduction reaction, the reaction formula is: $O_2 + e^- + H^+ \rightarrow$ •OOH, •OOH + $e^- + H^+ \rightarrow H_2O_2$ (II); $OH^- + OH^- \rightarrow H_2O_2$ (III).

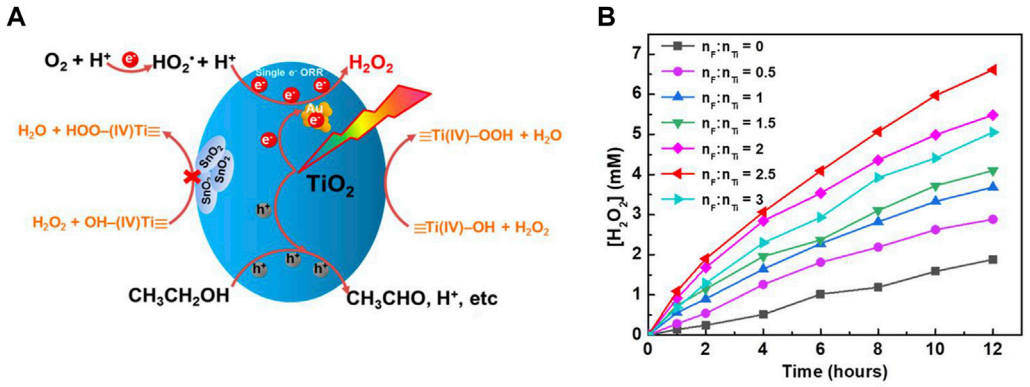

FIGURE 3
(A) Schematic illustration of H_2O_2 synthesis and decomposition over Au/SnO_2 -TiO_2 (Zuo et al., 2019b). **(B)** Photocatalytic H_2O_2 production over 0.1% Au/F-TiO_2 prepared with different F/Ti ratios (Li L. et al., 2021).

(Zheng et al., 2018; Zhang M. M. et al., 2020; Liu et al., 2021a). Table 1 summarizes the effects of cocatalysts on hydrogen peroxide production activity.

3 Effect of surface modification on photocatalytic activity

In addition to increasing the activity of H_2O_2 production by the deposition of co-catalysts, decreasing the decomposition rate *via* surface modification is essential to maximize the final concentration of H_2O_2.

3.1 Surface passivation modification

TiO_2 can catalyze the decomposition of H_2O_2 under visible light. Ti-OOH that form on the surface due to the interaction of TiO_2 and H_2O_2 gradually degrade under visible light. This is the main reason for the decrease of H_2O_2 concentration during reactions (Li et al., 2001; Teranishi et al., 2010). Surface passivation can effectively inhibit the decomposition of H_2O_2. It can be carried out either by metal oxide passivation or non-metal passivation. Passivation of a photocatalyst with a metal oxide leads to the formation of a heterojunction (Zeng et al., 2017; Zuo et al., 2019b; Awa et al., 2020; Feng et al., 2021). For example, the surface of anatase TiO_2 and rutile TiO_2 were modified with SnO_2 to form SnO_2-TiO_2 heterojunction. Then, the surface was functionalized with gold nanoparticles, and it was found that the formation activity of H_2O_2 was improved. This is because the decomposition of H_2O_2 on the TiO_2 surface is inhibited (Figure 3A) (Zuo et al., 2019b). However, the H_2O_2 photocatalytic synthesis reaction rate of Au modified Bi_2O_3-TiO_2 was better than that of Au/SnO_2-TiO_2. This is because not only the decomposition of H_2O_2 is inhibited, but also the carrier recombination in Bi_2O_3 is inhibited (Feng et al., 2021). A similar phenomenon is found in the heterojunction formed on g-C_3N_4 (Chen et al., 2017b; Chen X. L. et al., 2020; Liu et al., 2021b).

Non—metallic surface modification was also effective for improving photocatalytic activity (Maurino et al., 2005; Moon et al., 2014; Zhang M. M. et al., 2020; Li L. et al., 2021). For example, by hydrothermal treatment of TiO_2 and NaF to obtain F-TiO_2, the decomposition of H_2O_2 is inhibited. This was due to the fact that the F ion fixed on the TiO_2 surface competes with the Ti-OOH formation, thus reducing the Ti-OOH formation. Therefore, it was no longer necessary to add NaF to the photocatalytic reaction medium (Figure 3B) (Li L. et al., 2021).

3.2 Organic molecular modification

Imine organic molecules can be used to modify the surface of g-C_3N_4 to inhibit the electron-hole pair recombination of g-C_3N_4 (Shiraishi et al., 2014a; Kofuji et al., 2016; Yang et al., 2017; Goclon and Winkler, 2018; Guo et al., 2020; Zeng et al., 2020). For example, modification of the surface of g-C_3N_4 with homobendiimide and bibendiimide increased the synthesis activity of H_2O_2 (Figures 4A–C) (Shiraishi et al., 2014a; Kofuji et al., 2016). Besides the pure g-C_3N_4 reaction, another H_2O_2 synthesis pathway ($\bullet OH + \bullet OH \rightarrow H_2O_2$) also plays a key role in the polyimide modified g-C_3N_4 nanosheets (Yang et al., 2017). In another publication, it was found that the modification of g-C_3N_4 by β-cyclodextrin can increase its hydrophobicity and affinity for oxygen, thus increasing the yield of H_2O_2 (Figure 4D) (Zuo et al., 2020).

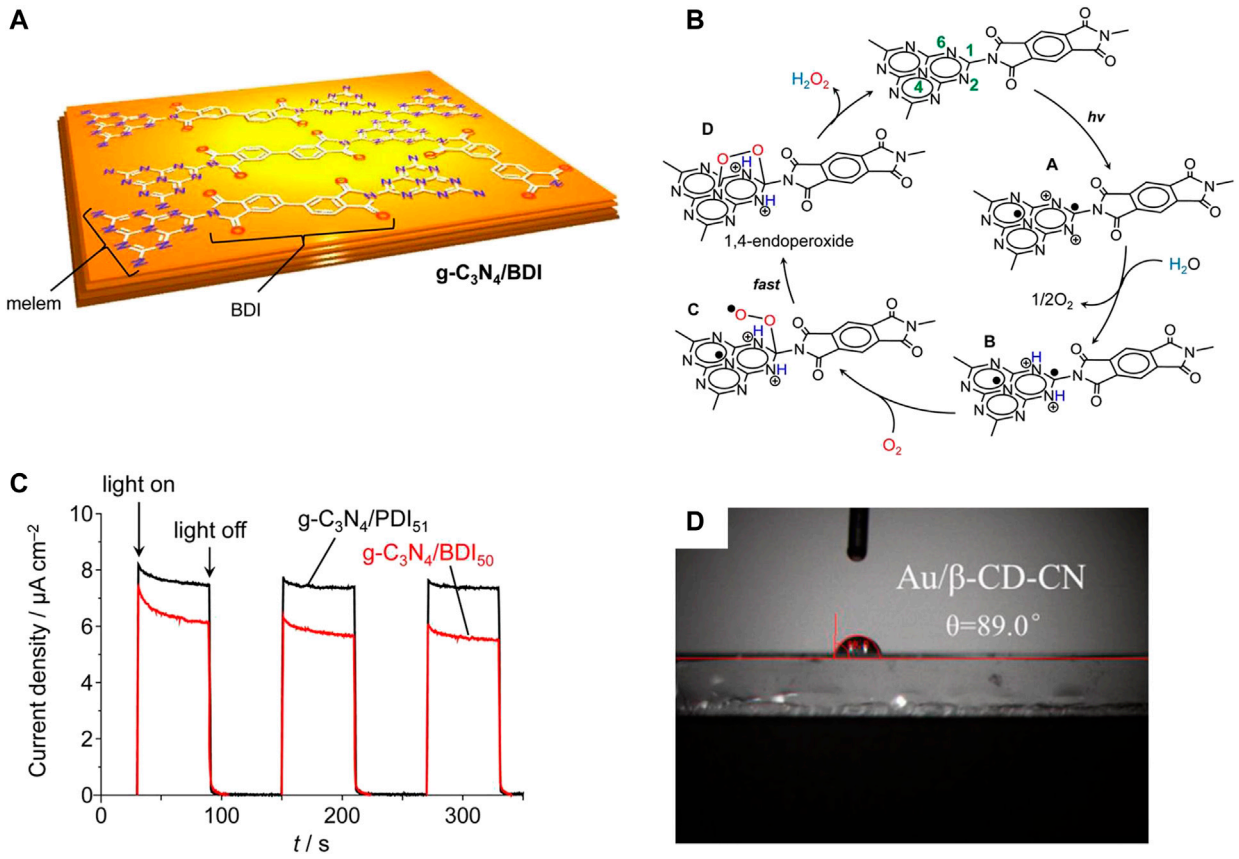

FIGURE 4
(A) Three-dimensional structure of g-C_3N_4/BDI. **(B)** Proposed Mechanism for H_2O_2 Formation on the Photoexcited g-C_3N_4/BDI Catalyst. **(C)** Photocurrent response of g-C_3N_4/BDI_{50} and g-C_3N_4/PDI_{51} in 0.1 M Na_2SO_4 solution under visible light (λ >420 nm) at a bias of 0.5 V vs. Ag/AgCl (Kofuji et al., 2016). **(D)** The water contact angle of Au/β-CD-CN (Zuo et al., 2020).

Metal organic frameworks (MOFs) are promising materials that can be used to modify photocatalysts. This is because metal nodes and organic linkers of MOFs can be easily modified to improve photon absorption and catalytic activity. Therefore, various modification strategies have been devised, such as double substrate metal-organic framework, metal nanoparticles and MOF composite, etc (Wang Z. et al., 2020; Duan et al., 2020; Younis et al., 2020; Fang et al., 2021). The results showed that the activity of H_2O_2 synthesis was improved by modification of ZIF (Chang et al., 2020) and MIL (Isaka et al., 2019) type metal-organic framework materials. It was mainly attributed to the wider bandgap energy. Titanium-zirconium MOFs were prepared and used for photocatalytic production of H_2O_2 in two phase system (water/benzoic acid). Ti species effectively promoted electron transfer from the photoexcited linkers of MOFs to Ti and inhibited the recombination of electron-hole pairs in the hydrophobic MOFs matrix (Chen et al., 2020c). Table 2 summarizes the effects of different surface modifications on hydrogen peroxide production activity.

4 Effect of doping on the photocatalytic activity

Doping elements can effectively reduce the band gap of photocatalysts to improve the utilization of solar light (Akpan and Hameed, 2010; Zhao et al., 2017). Studies have shown that doping can change the number of active sites, reduce the formation energy of •OOH intermediates, and promote the formation of H_2O_2 (Li X. et al., 2021). Therefore, incorporating metal and non-metal ions in the photocatalyst can improve the photocatalytic synthesis activity of H_2O_2 (Table 3).

4.1 Metal ion incorporation

Incorporating metal ions in the photocatalyst can improve the photocatalytic synthesis activity of H_2O_2 (Wu et al., 2017; Kim S. et al., 2018; Qu et al., 2018; Feng et al., 2020; Hu et al.,

TABLE 2 Activities of photocatalysts with different types of surface modification.

Photocatalyst	Catalyst mass	Incident light	Load	Reaction condition	H_2O_2 activity	Function of modification	Reaction mechanism*	References
M_V-M_S-CN/MAFO	0.2 g (200 ml)	250 W high-pressure sodium lamp (400–800 nm)	n_{Mg}: n_{Al}: n_{Fe} = 5 : 2: 1	O_2, 0.5 mol L^{-1} $NaNO_2$	6.3 mmol L^{-1} (18 h)	Surface passivation modification	(I)	Chen et al. (2017b)
Au/SnO_2-NR#TiO_2	10 mg (10 ml)	300 W Xe lamp (λ > 430 nm)	—	O_2, 4% EtOH	60 μM (6 h)	Surface passivation modification	(I)	Awa et al. (2020)
F/TiO_2(P25)	0.5 g/L	40 W fluorescent lamp (λ > 360 nm)	F 1.0 × 10^{-2} M	pH = 3.2, Air, 1.0 × 10^{-2} M HCOOH	1.3 × 10^{-3} mol•L^{-1} (100 min)	Surface passivation modification	(II)	Maurino et al. (2005)
Au/SnO_2-TiO_2	0.2 g (200 ml)	300 W Xe arc lamp	Au 0.1 wt % n_{Sn}: n_{Ti} = 4%	O_2, 4% EtOH	9 mM (12 h)	Surface passivation modification	(II)	Zuo et al. (2019b)
TiO_2/rGO/WO_3(TRW)	3 mg (30 ml)	200 W arc Mercury-Xenon research lamp	Na_2WO_4 0.5 M	—	350 μM (80 min)	Surface passivation modification	(I)	Zeng et al. (2017)
rGO/TiO_2/P	0.5 g/L	λ > 320 nm	rGO 6 wt %, 0.1 M of phosphate buffer	Ph = 3, O_2, 5 vol% IPA	4.5 mM (200 min)	Surface passivation modification	—	Moon et al. (2014)
HTNT-CD	20 mg (15 ml)	350 W Xe lamp (λ > 365 nm)	CDs 2.6 wt%	Air	3.42 mmol $gcat^{-1}$ h^{-1}	Quantum dots	(I) (III)	Ma et al. (2019)
g-C_3N_4/BDI	100 mg (30 ml)	λ > 420 nm	melem: BTCDA (mol: mol) = 1::2.5	O_2, 10 vol% 2-PrOH	41 μmol (48 h)	Organic molecular modification	(I)	Kofuji et al. (2016)
g-C_3N_4/PDI	50 mg (30 ml)	Xe lamp (λ > 420 nm)	—	O_2	50.6 μmol (48 h)	Organic molecular modification	(II)	Shiraishi et al. (2014a)
RF523 @333 K	50 mg (30 ml)	Xe lamp (λ > 420 nm)	—	O_2	100 μmol (24 h)	Organic molecular modification	(I)	Shiraishi et al. (2019)
PCNBA0.2	50 mg (30 ml)	500 W Xe lamp (λ > 420 nm)	melem: BA = 3 g: 0.2 g	O_2	>2 mg/L (1 h)	Organic molecular modification	(II)	Teng et al. (2020)
rGO/Cd_3 $(TMT)_2$	80 mg (20 ml)	λ > 420 nm	rGO 0.1 wt%	O_2, 5 vol% MeOH	7 mmol•L^{-1} (24 h)	Organic molecular modification	(II)	Xu et al. (2017)
PI-NCN	50 mg (50 ml)	300 W Xe lamp (λ > 420 nm)	PI 5 wt%	—	120 μmol (120 min)	Organic molecular modification	(II) (III)	Yang et al. (2017)
PEI/C_3N_4	20 mg (20 ml)	arc Xenon research lamp (Newport) with AM 1.5 air filter	PEI 50% W/V	O_2	208.1 μM (60 min)	Organic molecular modification	(II)	Zeng et al. (2020)
MIL-125-R7	5 mg (7 ml)	λ > 420 nm	caprylic anhydride treatment	BA/H_2O = 5ml/2 ml	1500 μM (2 h)	MOF	(II)	Isaka et al. (2019)

(Continued on following page)

TABLE 2 (*Continued*) Activities of photocatalysts with different types of surface modification.

Photocatalyst	Catalyst mass	Incident light	Load	Reaction condition	H_2O_2 activity	Function of modification	Reaction mechanism*	References
ZIF-8	0.05 g (100 ml)	350 W Xenon lamp	—	O_2, water	75 μmol•L^{-1}•h^{-1}	MOF	—	Chang et al. (2020)
OPA/$Zr_{100-x}Ti_x$-MOF	5 mg (7 ml)	500 W Xe lamp (λ > 420 nm)	Ti: (Ti + Zr) (mol: mol) = 7.5%	O_2, BA/H_2O = 5ml/2 ml	9.7 mmol•L^{-1}•h^{-1}	MOF	(II)	Chen et al. (2020c)

*The reaction mechanism is direct two electron oxygen reduction reaction, The reaction formula is: $O_2 + 2e^- + 2H^+ \rightarrow H_2O_2$ (I); Step by step one electron oxygen reduction reaction, the reaction formula is: $O_2 + e^- + H^+ \rightarrow$ •OOH, •OOH + $e^- + H^+ \rightarrow H_2O_2$ (II); $OH^- + OH^- \rightarrow H_2O_2$ (III).

TABLE 3 Activities of photocatalysts with different types of ion doping.

Photocatalyst	Catalyst mass	Incident light	Load	Reaction condition	H_2O_2 activity	Reaction pathway*	References
KBH_4/g-C_3N_4	50 mg (100 ml)	300 W Xe lamp (λ > 420 nm)	KBH_4 0.17 wt%	O_2, 10 vol% IPA	287 μmol h^{-1}	(II)	Feng et al. (2020)
KPF_6-CN	0.5 g/L	300 W Xe lamp (λ > 420 nm)	15 mmol KPF_6	Ph = 3, O_2, 10 vol % EtOH	1.5 mM (5 h)	(I)	Kim et al. (2018c)
Cv-g-C_3N_4	0.1 g (100 ml)	300 W Xe lamp (λ > 420 nm)	—	O_2	90 μM (60 min)	(I)	Li et al. (2016)
K^+-Na^+/g-C_3N_4	0.2 g (200 ml)	250 W high-pressure sodium lamp (400–800 nm)	K^+ 1.3 wt%, Na^+ 0.7 wt%	O_2, $NaNO_2$ (0.5 mol L^{-1})	4.6 mmol L^{-1} (18 h)	(I) (III)	Qu et al. (2018)
Pt-KCN	0.2 g (200 ml)	250 W high-pressure sodium lamp (400–800 nm)	Pt 1 wt%, 5 ml KOH (0.1 mol/L)	Remove the air	620 μmol •g^{-1}	(II)	Hu et al. (2020)
K_2HPO_4/GCN	0.1 g (100 ml)	300 W Xe lamp (λ > 420 nm)	Urea (g): Dopant (mmol) = 10 : 10	O_2, 10 vol% EtOH	5.05 mM (10 h)	(I)	Tian et al. (2019)
OCN(24)	0.2 g (200 ml)	250 W high-pressure sodium lamp (400–800 nm)	—	O_2, 0.5 mol L^{-1} $NaNO_2$	3.8 mmol L^{-1} (12 h)	(I) (III)	Wang et al. (2019a)
Ni-FCN	0.2 g (200 ml)	250 W high-pressure sodium lamp (400–800 nm)	n_{Ni}/dicyandiamide = 0.006	O_2	7.7 mmol L^{-1} (12 h)	(I)	Wu et al. (2017)
KPD-CN	20 mg (40 ml)	300 W Xe lamp (λ > 420 nm)	Urea (g): Dopant (mmol) = 4 : 7.5	pH = 3, O_2, 10 vol% EtOH	1.5 mM (7 h)	(I)	Moon et al. (2017)
rGO/TiO_2/P	0.5 g/L	λ > 320 nm	rGO 6 wt%, 0.1 M of phosphate buffer	Ph = 3, O_2, 5 vol % IPA	4.5 mM (200 min)	—	Moon et al. (2014)
OCN-500	—	λ > 420 nm	—	O_2, 10 vol% IPA	730 μmol (5 h)	(I)	Wei et al. (2018)
AQ/U-POCN	10 mg (20 ml)	300 W Xe lamp (400–780 nm)	U-POCN: AQ = 12 μM: 4 μM	Air	75 μM h^{-1}	(II)	Ye et al. (2021)
Br-H-GCN	0.2 g (200 ml)	250 W high-pressure sodium lamp (400–800 nm)	Br 0.75 wt%	O_2, 0.15g EDTA	1.99 mmol L^{-1} (5 h)	(I)	Zhang et al. (2018)

*The reaction mechanism is direct two electron oxygen reduction reaction, The reaction formula is: $O_2 + 2e^- + 2H^+ \rightarrow H_2O_2$ (I); Step by step one electron oxygen reduction reaction, the reaction formula is: $O_2 + e^- + H^+ \rightarrow$ •OOH, •OOH + $e^- + H^+ \rightarrow H_2O_2$ (II); $OH^- + OH^- \rightarrow H_2O_2$ (III).

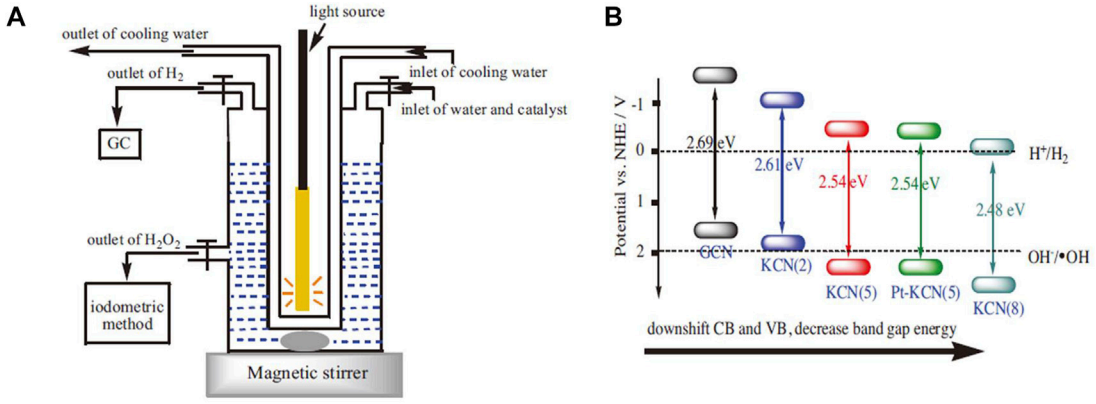

FIGURE 5
(A) The schematic diagram of the reactor. **(B)** The band position of $K^+/g\text{-}C_3N_4$ (Hu et al., 2020).

2020). For example, incorporating $g\text{-}C_3N_4$ with K^+ can be used to photocatalyze water decomposition to produce H_2 and H_2O_2 simultaneously without any sacrificial agent (Figure 5A). K^+ was coordinated into the big C-N rings by forming the N-bridge, which inhibits the crystal growth of $g\text{-}C_3N_4$, promotes the specific surface area, increases the visible light absorption. More importantly, the CB and VB can be adjusted to the best position (Figure 5B) (Hu et al., 2020). A similar phenomenon of band gap adjustment was observed in $g\text{-}C_3N_4$ co-incorporated with $K^+$and Na^+. After the band gap adjustment, not only CB electrons can reduce O_2 to produce H_2O_2, but also VB holes can oxidize OH^- to •OH for H_2O_2 synthesis. This made the generation mechanism of photocatalytic H_2O_2 change from "single channel pathway" ($O_2 + 2e^- + 2H^+ \rightarrow H_2O_2$) to "dual channel pathway" ($O_2 + 2e^- + 2H^+ \rightarrow H_2O_2$ and $•OH+•OH \rightarrow H_2O_2$ reaction pathways) (Qu et al., 2018).

4.2 Non-metal ion doping

Non-metal ion doping photocatalyst can effectively improve the synthetic activity of H_2O_2 (Moon et al., 2014; Wei et al., 2018; Zhang et al., 2018; Wang L. C. et al., 2019; Ye et al., 2021). For example, halogens (Cl and Br) were incorporated into $g\text{-}C_3N_4$ by hydrothermal method (Figure 6A), and it was found that $g\text{-}C_3N_4$ incorporated with Br was more conducive to H_2O_2 synthesis. This is mainly due to the larger specific surface area and higher charge separation rate after incorporating (Figure 6B) (Zhang et al., 2018). A similar phenomenon was observed in the co-doping of metal ions and non-metals (K and P) (Figure 6C). Compared with $g\text{-}C_3N_4$ incorporated with P ($NH_4H_2PO_4$/GCN) or K^+ (K_2SO_4/GCN), the H_2O_2 generation of $g\text{-}C_3N_4$ after co-incorporating was 10.98 times of the former and 5.2 times of the latter, respectively (Figure 6D) (Tian et al., 2019). Similarly, co-doping can also improve the catalytic activity of TiO_2. For example, Fe and S were co-doped into TiO_2 by one-step anodic oxidation, and it was found that the synthesis activity of TiO_2 was improved after doping. This is mainly attributed to the fact that Fe-S co doped TiO_2 had a narrower band gap than pure TiO_2, resulting in a wider visible light absorption range (Momeni and Akbarnia, 2021).

5 Effect of reaction environment on photocatalytic activity

5.1 Effects of temperature and pH

One study investigated the effect of temperature and pH on the photoactivity of H_2O_2 generation by using Au/TiO_2 photocatalyst. The results showed that when pH value (pH = 2) or temperature (5°C) was low, it was more beneficial to improve the photoactivity. The main reason was that the thermal catalytic decomposition of H_2O_2 by Au/TiO_2 can be effectively inhibited at low pH value or low temperature (Teranishi et al., 2016). In another study, it was found that low pH also increased the H_2O_2 synthesis activity of MOFs materials. At the same temperature, when the pH value of MOFs material was as low as 0.3, the formation of H_2O_2 was more favorable. (Isaka et al., 2019).

5.2 Effects of sacrificial agents

For the photocatalytic production of H_2O_2, a certain amount of sacrificial agent is usually added to act as hole scavenger and prevent the recombination of electron–hole pairs. The sacrificial agents were mainly alcohols, which provided hydrogen source for photocatalytic H_2O_2 generation (Kormann et al.). However, the ability of aliphatic alcohols (such as ethanol and methanol, which

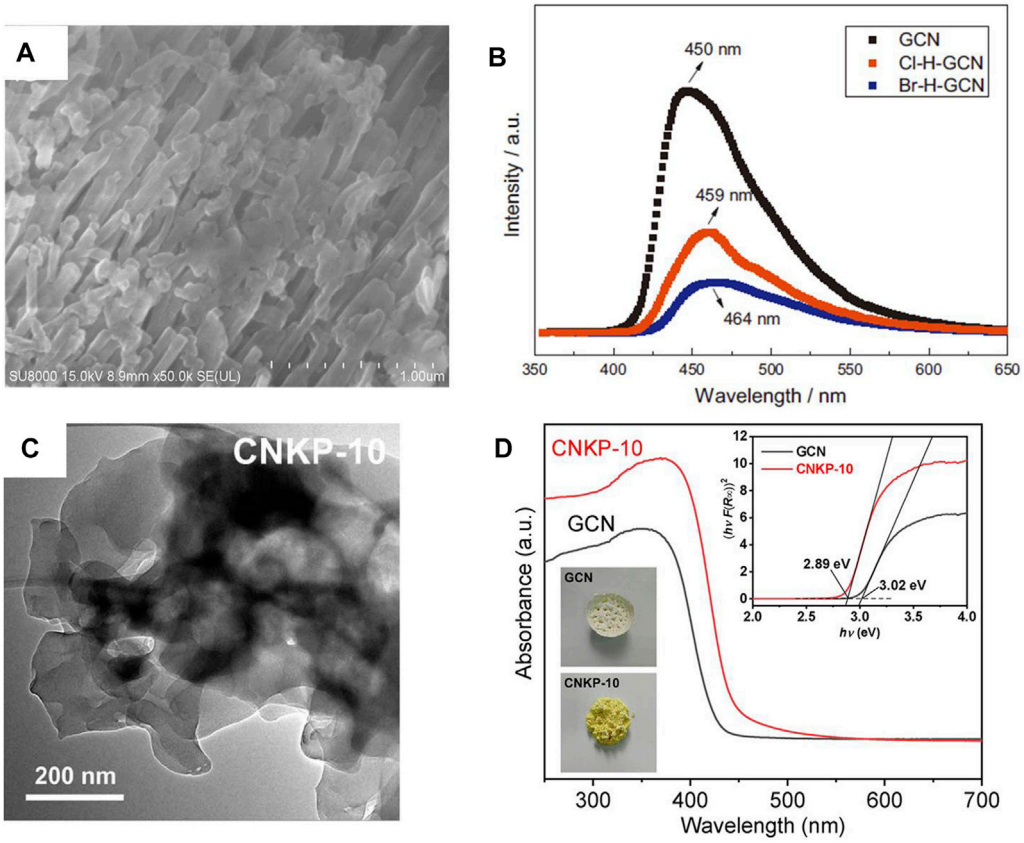

FIGURE 6
(A) The SEM images of Br-H-GCN. **(B)** PL spectra of GCN, Cl-H-GCN and Br-H-GCN (Zhang et al., 2018). **(C)** TEM images of the CNKP-10 catalysts. **(D)** UV–vis DRS spectra of the GCN and CNKP-10 catalysts (Tian et al., 2019).

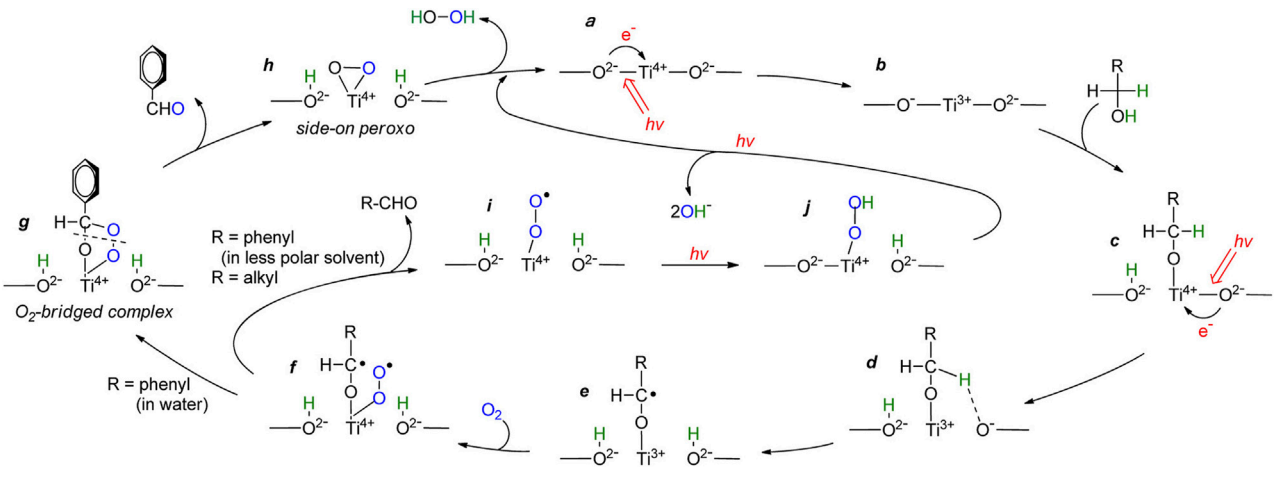

FIGURE 7
Proposed mechanism for photocatalytic oxidation of alcohols with O_2 on the TiO_2 Surface (Shiraishi et al., 2013).

act as electron donors) to improve photoactivity is limited. The results showed that g-C_3N_4 can effectively synthesize H_2O_2 in deionized water containing oxygen under visible light irradiation. This was due to the efficient formation of 1, 4-endoperoxide on the surface of g-C_3N_4. The addition of ethanol inhibited the one-electron reduction of O_2 (formation of superoxide radicals) and selectively promoted the two-electron reduction of O_2. At the same time, the photodecomposition of hydrogen peroxide formed subsequently was inhibited (Shiraishi et al., 2014b). Kim et al, (2016) also investigated whether the addition of electron donors affects photocatalytic activity. The results showed that when no sacrificial agent (methanol) was added to the system, the generation activity of H_2O_2 was extremely low. This result confirmed that using sacrificial agents such as methanol is important. When methanol (5 vol%) was present in the system, H_2O_2 was generated together with formaldehyde ($CH_3OH + O_2 \rightarrow HCHO + H_2O_2$). Meanwhile, ethanol and 2-propanol were tested further, and the results showed that these alcohols worked effectively as electron donors.

However, aliphatic alcohols (such as ethanol and methanol) as electron donors have limited improvement in photocatalytic activity for hydrogen peroxide synthesis. Therefore, some studies have tried to use aromatic alcohol (benzyl alcohol) as a sacrifice agent, compared with fatty alcohol. The results showed that, during photoreaction with aliphatic alcohol, the carbon radical was rapidly removed and leaved superoxo radical (the f→i process in Figure 7), resulting in very low for H_2O_2 formation. In the aqueous phase containing benzyl alcohol, the carbon free radical was stably transformed into an oxygen bridge complex (f→g→h process in Figure 7), which generates a large number of peroxides and improves the synthesis activity of H_2O_2. The results showed that benzyl alcohol as electron donor can improve the reactivity. (Shiraishi et al., 2013).

Conclusions and outlook

In future, the photocatalytic H_2O_2 synthesis system still need to improve the reaction activity and sustainability. We should consistently increase the upper limit of H_2O_2 production concentration in long-term photocatalytic reaction. The kinetics of photocatalytic H_2O_2 decomposition should be especially concerned. It is also urgent to develop efficient non-precious cocatalysts with two-electron ORR selectivity.

The activity of H_2O_2 synthesis was very unsatisfactory in most pure water systems. As a compromise for adding sacrificial reagents, the photocatalytic H_2O_2 synthesis system could be coupled with other valuable photocatalytic selective oxidation reaction to maximize its value, such as coupling with selective oxidation or photocatalytic degradation reactions.

Author contributions

Conceptualization, XM, XX, and JZ; writing—original draft preparation, HW, and SH; writing—review and editing, XM and VR; funding acquisition, XM. HW and SH contributed equally to this work. All authors have read and agreed to the published version of the manuscript.

Funding

This work received financial support from the National Natural Science Foundation of China (51872091), the Natural Science Foundation of Hebei Province (H2022209089), Basic Scientific Research Expenses of Universities in Hebei Province (JYG2021003 and JYG 2022001), and Tangshan Talent Funding Project (A202202007).

Conflict of interest

The authors declare that the research was conducted in the absence of any commercial or financial relationships that could be construed as a potential conflict of interest.

Publisher's note

All claims expressed in this article are solely those of the authors and do not necessarily represent those of their affiliated organizations, or those of the publisher, the editors and the reviewers. Any product that may be evaluated in this article, or claim that may be made by its manufacturer, is not guaranteed or endorsed by the publisher.

References

Adams, J. S., Kromer, M. L., Rodriguez-Lopez, J., and Flaherty, D. W. (2021). Unifying concepts in electro- and thermocatalysis toward hydrogen peroxide production. *J. Am. Chem. Soc.* 143, 7940–7957. doi:10.1021/jacs.0c13399

Akpan, U. G., and Hameed, B. H. (2010). The advancements in sol–gel method of doped-TiO_2 photocatalysts. *Appl. Catal. A General* 375, 1–11. doi:10.1016/j.apcata.2009.12.023

Anantharaj, S., Pitchaimuthu, S., and Noda, S. (2021). A review on recent developments in electrochemical hydrogen peroxide synthesis with a critical assessment of perspectives and strategies. *Adv. Colloid Interface Sci.* 287, 102331. doi:10.1016/j.cis.2020.102331

Andersen, B. M., Rasch, M., Hochlin, K., Jensen, F. H., Wismar, P., and Fredriksen, J. E. (2006). Decontamination of rooms, medical equipment and ambulances using an aerosol of hydrogen peroxide disinfectant. *J. Hosp. Infect.* 62, 149–155. doi:10.1016/j.jhin.2005.07.020

Apaydin, D. H., Seelajaroen, H., Pengsakul, O., Thamyongkit, P., Sariciftci, N. S., Kunze-Liebhauser, J., et al. (2018). Photoelectrocatalytic synthesis of hydrogen

peroxide by molecular copper-porphyrin supported on titanium dioxide nanotubes. *ChemCatChem* 10, 1793–1797. doi:10.1002/cctc.201702055

Awa, K., Naya, S.-I., Fujishima, M., and Tada, H. (2020). A three-component plasmonic photocatalyst consisting of gold nanoparticle and TiO_2–SnO_2 nanohybrid with heteroepitaxial junction: Hydrogen peroxide synthesis. *J. Phys. Chem. C* 124, 7797–7802. doi:10.1021/acs.jpcc.9b11875

Baran, T., Wojtyla, S., Vertova, A., Minguzzi, A., and Rondinini, S. (2018). Photoelectrochemical and photocatalytic systems based on titanates for hydrogen peroxide formation. *J. Electroanal. Chem.* 808, 395–402. doi:10.1016/j.jelechem.2017.06.044

Cai, J., Huang, J., Wang, S., Iocozzia, J., Sun, Z., Sun, J., et al. (2019). Crafting mussel-inspired metal nanoparticle-decorated ultrathin graphitic carbon nitride for the degradation of chemical pollutants and production of chemical resources. *Adv. Mater* 31, e1806314. doi:10.1002/adma.201806314

Campos-Martin, J. M., Blanco-Brieva, G., and Fierro, J. L. (2006). Hydrogen peroxide synthesis: An outlook beyond the anthraquinone process. *Angew. Chem. Int. Ed. Engl.* 45, 6962–6984. doi:10.1002/anie.200503779

Chang, A. L., Nguyen, V. H., Lin, K. Y. A., and Hu, C. C. (2020). Selective synthesis of ZIFs from zinc and nickel nitrate solution for photocatalytic H_2O_2 production. *Arabian J. Chem.* 13, 8301–8308. doi:10.1016/j.arabjc.2020.04.027

Chang, S. L., Li, H., Liu, J. N., Zhao, M. X., Tan, M. H., Xu, P. W., et al. (2021). Effect of hydrogen peroxide treatment on the quality of epsilon-poly-L-lysine products. *Biochem. Eng. J.* 171, 108017. doi:10.1016/j.bej.2021.108017

Chang, X. Y., Yang, J. J., Han, D. D., Zhang, B., Xiang, X., and He, J. (2018). Enhancing light-driven production of hydrogen peroxide by anchoring Au onto C_3N_4 catalysts. *Catalysts* 8, 147. doi:10.3390/catal8040147

Chen, J. Y., Cao, J. M., Zhou, J., Wang, W. Q., Zhang, Y. F., Liu, J. F., et al. (2020a). A computational evaluation of MoS_2-based materials for the electrocatalytic oxygen reduction reaction. *New J. Chem.* 44, 14189–14197. doi:10.1039/d0nj02621b

Chen, Q. (2008). Development of an anthraquinone process for the production of hydrogen peroxide in a trickle bed reactor—from bench scale to industrial scale. *Chem. Eng. Process. Process Intensif.* 47, 787–792. doi:10.1016/j.cep.2006.12.012

Chen, S., Tu, R., Li, J., and Lu, X. (2018). Pd catalysts supported on rGO-TiO_2 composites for direct synthesis of H_2O_2 : Modification of Pd^{2+}/Pd^0 ratio and hydrophilic property. *Chin. J. Chem. Eng.* 26, 534–539. doi:10.1016/j.cjche.2017.07.016

Chen, X., Hu, S. Z., Li, P., Li, W., Ma, H. F., and Lu, G. (2017). Photocatalytic production of hydrogen peroxide using g-C_3N_4 coated MgO-Al_2O_3-Fe_2O_3 heterojunction catalysts prepared by a novel molten salt-assisted microwave process. *Acta Physico-Chimica Sin.* 33, 2532–2541. doi:10.3866/pku.Whxb201706153

Chen, X. L., Kuwahara, Y., Mori, K., Louis, C., and Yamashita, H. (2020b). A hydrophobic titanium doped zirconium-based metal organic framework for photocatalytic hydrogen peroxide production in a two-phase system. *J. Mater. Chem. A* 8, 1904–1910. doi:10.1039/c9ta11120d

Chen, X., Zhang, W., Zhang, L., Feng, L., Zhang, C., Jiang, J., et al. (2020). Sacrificial agent-free photocatalytic H_2O_2 evolutionviatwo-electron oxygen reduction using a ternary α-Fe_2O_3/CQD@g-C_3N_4 photocatalyst with broad-spectrum response. *J. Mater. Chem. A* 8, 18816–18825. doi:10.1039/d0ta05753c

Chen, Y. M., Gu, W. Q., Tan, L., Ao, Z. M., An, T. C., and Wang, S. B. (2021). Photocatalytic H_2O_2 production using Ti_3C_2 MXene as a non-noble metal cocatalyst. *Appl. Catal. a-General* 618, 118127. doi:10.1016/j.apcata.2021.118127

Chen, Z., Li, C., Ni, Y., Kong, F., Kong, A., and Shan, Y. (2017). Ag-Enhanced catalytic performance of ordered mesoporous Fe–N-graphitic carbons for oxygen electroreduction. *Catal. Lett.* 147, 2745–2754. doi:10.1007/s10562-017-2186-2

Chung, S., Chung, J., and Chung, C. (2020). Enhanced electrochemical oxidation process with hydrogen peroxide pretreatment for removal of high strength ammonia from semiconductor wastewater. *J. Water Process Eng.* 37, 101425. doi:10.1016/j.jwpe.2020.101425

Dinakar, M., Tao, W. D., and Daley, D. (2020). Using hydrogen peroxide to supplement oxygen for nitrogen removal in constructed wetlands. *J. Environ. Chem. Eng.* 8, 104517. doi:10.1016/j.jece.2020.104517

Du, L., Zhang, G. X., Liu, X. H., Hassanpour, A., Dubois, M., Tavares, A. C., et al. (2020). Biomass-derived nonprecious metal catalysts for oxygen reduction reaction: The demand-oriented engineering of active sites and structures. *Carbon Energy* 2, 561–581. doi:10.1002/cey2.73

Duan, M. B., Jiang, L. B., Zeng, G. M., Wang, D. B., Tang, W. W., Liang, J., et al. (2020). Bimetallic nanoparticles/metal-organic frameworks: Synthesis, applications and challenges. *Appl. Mater. Today* 19, 100564. doi:10.1016/j.apmt.2020.100564

Edwards, J. K., and Hutchings, G. J. (2008). Palladium and gold-palladium catalysts for the direct synthesis of hydrogen peroxide. *Angew. Chem. Int. Ed. Engl.* 47, 9192–9198. doi:10.1002/anie.200802818

Fang, Y., Yang, Y., Yang, Z. G., Li, H. P., and Roesky, H. W. (2021). Advances in design of metal-organic frameworks activating persulfate for water decontamination. *J. Organomet. Chem.* 954, 122070. doi:10.1016/j.jorganchem.2021.122070

Feng, C. Y., Tang, L., Deng, Y. C., Wang, J. J., Luo, J., Liu, Y. N., et al. (2020). Synthesis of leaf-vein-like g-C(3)N(4)with tunable band structures and charge transfer properties for selective photocatalytic H(2)O(2)Evolution. *Adv. Funct. Mater.* 30, 2001922. doi:10.1002/adfm.202001922

Feng, L. W., Li, B. D., Xiao, Y. Q., Li, L. J., Zhang, Y. Q., Zhao, Q. N., et al. (2021). Au modified Bi_2O_3-TiO_2 hybrid for photocatalytic synthesis of hydrogen peroxide. *Catal. Commun.* 155, 106315. doi:10.1016/j.catcom.2021.106315

Fukuzumi, S., Lee, Y. M., and Nam, W. (2018). Solar-Driven production of hydrogen peroxide from water and dioxygen. *Chemistry* 24, 5016–5031. doi:10.1002/chem.201704512

Gao, G. H., Tian, Y. N., Gong, X. X., Pan, Z. Y., Yang, K. Y., and Zong, B. N. (2020). Advances in the production technology of hydrogen peroxide. *Chin. J. Catal.* 41, 1039–1047. doi:10.1016/S1872-2067(20)63562-8

Goclon, J., and Winkler, K. (2018). Computational insight into the mechanism of O_2 to H_2O_2 reduction on amino-groups-containing g-C_3N_4. *Appl. Surf. Sci.* 462, 134–141. doi:10.1016/j.apsusc.2018.08.070

Guarino, V. A., Oldham, W. M., Loscalzo, J., and Zhang, Y. Y. (2019). Reaction rate of pyruvate and hydrogen peroxide: Assessing antioxidant capacity of pyruvate under biological conditions. *Sci. Rep.* 9, 19568. doi:10.1038/s41598-019-55951-9

Guo, F., Zhang, M., Yi, S., Li, X., Xin, R., Yang, M., et al. (2022). Metal-coordinated porous polydopamine nanospheres derived Fe_3N-FeCo encapsulated N-doped carbon as a highly efficient electrocatalyst for oxygen reduction reaction. *Nano Res. Energy* 1, e9120027. doi:10.26599/NRE.2022.9120027

Guo, Y., Li, H. R., Ma, W., Shi, W. X., Zhu, Y. F., and Choi, W. Y. (2020). Photocatalytic activity enhanced via surface hybridization. *Carbon Energy* 2, 308–349. doi:10.1002/cey2.66

Haider, Z., Cho, H. I., Moon, G. H., and Kim, H. I. (2019). Minireview: Selective production of hydrogen peroxide as a clean oxidant over structurally tailored carbon nitride photocatalysts. *Catal. Today* 335, 55–64. doi:10.1016/j.cattod.2018.11.067

Halder, R., and Lawal, A. (2007). Experimental studies on hydrogenation of anthraquinone derivative in a microreactor. *Catal. Today* 125, 48–55. doi:10.1016/j.cattod.2007.03.055

Han, Y., He, Z. Y., Wang, S. L., Li, W., and Zhang, J. L. (2015). Performance of facet-controlled Pd nanocrystals in 2-ethylanthraquinone hydrogenation. *Catal. Sci. Technol.* 5, 2630–2639. doi:10.1039/c5cy00050e

Hirakawa, H., Shiota, S., Shiraishi, Y., Sakamoto, H., Ichikawa, S., and Hirai, T. (2016). Au nanoparticles supported on $BiVO_4$: Effective inorganic photocatalysts for H_2O_2 production from water and O_2 under visible light. *ACS Catal.* 6, 4976–4982. doi:10.1021/acscatal.6b01187

Hu, S., Sun, X., Zhao, Y., Li, W., Wang, H., and Wu, G. (2020). The effective photocatalytic water splitting to simultaneously produce H_2 and H_2O_2 over Pt loaded K-g-C_3N_4 catalyst. *J. Taiwan Inst. Chem. Eng.* 107, 129–138. doi:10.1016/j.jtice.2019.12.007

Ignaczak, A., Santos, E., and Schmickler, W. (2019). Oxygen reduction reaction on gold in alkaline solutions - the inner or outer sphere mechanisms in the light of recent achievements. *Curr. Opin. Electrochem.* 14, 180–185. doi:10.1016/j.coelec.2018.07.011

Isaka, Y., Kawase, Y., Kuwahara, Y., Mori, K., and Yamashita, H. (2019). Two-phase system utilizing hydrophobic metal-organic frameworks (MOFs) for photocatalytic synthesis of hydrogen peroxide. *Angew. Chem. Int. Ed. Engl.* 58, 5402–5406. doi:10.1002/anie.201901961

Jeon, T. Y., Yu, S. H., Yoo, S. J., Park, H. Y., and Kim, S. K. (2020). Electrochemical determination of the degree of atomic surface roughness in Pt–Ni alloy nanocatalysts for oxygen reduction reaction. *Carbon Energy* 3, 375–383. doi:10.1002/cey2.82

Jia, X. W., Sun, F., Fei, Y., Jin, M. P., Zhang, F., Xu, W., et al. (2018). Explosion characteristics of mixtures containing hydrogen peroxide and working solution in the anthraquinone route to hydrogen peroxide. *Process Saf. Environ. Prot.* 119, 218–222. doi:10.1016/j.psep.2018.08.007

Jirkovsky, J. S., Halasa, M., and Schiffrin, D. J. (2010). Kinetics of electrocatalytic reduction of oxygen and hydrogen peroxide on dispersed gold nanoparticles. *Phys. Chem. Chem. Phys.* 12, 8042–8052. doi:10.1039/c002416c

Jirkovsky, J. S., Panas, I., Ahlberg, E., Halasa, M., Romani, S., and Schiffrin, D. J. (2011). Single atom hot-spots at Au-Pd nanoalloys for electrocatalytic H_2O_2 production. *J. Am. Chem. Soc.* 133, 19432–19441. doi:10.1021/ja206477z

Kim, H. I., Choi, Y., Hu, S., Choi, W., and Kim, J. H. (2018b). Photocatalytic hydrogen peroxide production by anthraquinone-augmented polymeric carbon

nitride. *Appl. Catal. B-Environmental* 229, 121–129. doi:10.1016/j.apcatb.2018.01.060

Kim, H. I., Kwon, O. S., Kim, S., Choi, W., and Kim, J. H. (2016). Harnessing low energy photons (635 nm) for the production of H_2O_2 using upconversion nanohybrid photocatalysts. *Energy & Environ. Sci.* 9, 1063–1073. doi:10.1039/c5ee03115j

Kim, J., Kim, H. E., and Lee, H. (2018a). Single-atom catalysts of precious metals for electrochemical reactions. *ChemSusChem* 11, 104–113. doi:10.1002/cssc.201701306

Kim, S., Moon, G. H., Kim, H., Mun, Y., Zhang, P., Lee, J., et al. (2018c). Selective charge transfer to dioxygen on KPF_6-modified carbon nitride for photocatalytic synthesis of H_2O_2 under visible light. *J. Catal.* 357, 51–58. doi:10.1016/j.jcat.2017.10.002

Kofuji, Y., Ohkita, S., Shiraishi, Y., Sakamoto, H., Tanaka, S., Ichikawa, S., et al. (2016). Graphitic carbon nitride doped with biphenyl diimide: Efficient photocatalyst for hydrogen peroxide production from water and molecular oxygen by sunlight. *Acs Catal.* 6, 7021–7029. doi:10.1021/acscatal.6b02367

Kormann, C., Bahnemann, D. W., and Hoffmann, M. R. (1988). Photocatalytic production of hydrogen peroxides and organic peroxides in aqueous suspensions of titanium dioxide, zinc oxide, and desert sand. *Environ. Sci. Technol.* 22, 798–806. doi:10.1021/es00172a009

Kozlova, L. S., Novikov, V. T., Garaeva, G. R., Gol'din, M. M., and Kolesnikov, V. A. (2015). Electrodes modified with carbon materials in electrosynthesis of the dissolved hydrogen peroxide solutions and their medical properties. *Prot. Metals Phys. Chem. Surfaces* 51, 985–989. doi:10.1134/S2070205115060131

Li, L., Li, B., Feng, L., Zhang, X., Zhang, Y., Zhao, Q., et al. (2021a). Au modified F-TiO_2 for efficient photocatalytic synthesis of hydrogen peroxide. *Molecules* 26, 3844. doi:10.3390/molecules26133844

Li, S. N., Dong, G. H., Hailili, R., Yang, L. P., Li, Y. X., Wang, F., et al. (2016). Effective photocatalytic H_2O_2 production under visible light irradiation at g-C_3N_4 modulated by carbon vacancies. *Appl. Catal. B-Environmental* 190, 26–35. doi:10.1016/j.apcatb.2016.03.004

Li, X., Wang, X., Xiao, G., and Zhu, Y. (2021b). Identifying active sites of boron, nitrogen co-doped carbon materials for the oxygen reduction reaction to hydrogen peroxide. *J. Colloid Interface Sci.* 602, 799–809. doi:10.1016/j.jcis.2021.06.068

Li, X. Z., Chen, C. C., and Zhao, J. C. (2001). Mechanism of photodecomposition of H_2O_2 on TiO_2 surfaces under visible light irradiation. *Langmuir* 17, 4118–4122. doi:10.1021/la010035s

Liu, B., Bie, C., Zhang, Y., Wang, L., Li, Y., and Yu, J. (2021). Hierarchically porous ZnO/g-C_3N_4 S-scheme heterojunction photocatalyst for efficient H_2O_2 production. *Langmuir* 37, 14114–14124. doi:10.1021/acs.langmuir.1c02360

Liu, Y. M., Roy, S., Sarkar, S., Xu, J. Q., Zhao, Y. F., and Zhang, J. J. (2021). A review of carbon dots and their composite materials for electrochemical energy technologies. *Carbon Energy* 3, 795–826. doi:10.1002/cey2.134

Ma, R. Y., Wang, L., Wang, H., Liu, Z. Y., Xing, M. Y., Zhu, L. F., et al. (2019). Solid acids accelerate the photocatalytic hydrogen peroxide synthesis over a hybrid catalyst of titania nanotube with carbon dot. *Appl. Catal. B-Environmental* 244, 594–603. doi:10.1016/j.apcatb.2018.11.087

Maurino, V., Minero, C., Mariella, G., and Pelizzetti, E. (2005). Sustained production of H_2O_2 on irradiated TiO_2-fluoride systems. *Chem. Commun. (Camb)*, 2627–2629. doi:10.1039/b418789j

Meng, X. G., Zong, P. X., Wang, L., Yang, F., Hou, W. S., Zhang, S. T., et al. (2020). Au-nanoparticle-supported ZnO as highly efficient photocatalyst for H_2O_2 production. *Catal. Commun.* 134, 105860. doi:10.1016/j.catcom.2019.105860

Momeni, M. M., and Akbarnia, M. (2021). Photoelectrochemical, photocatalytic and electrochemical hydrogen peroxide production using Fe/S-codoped TiO_2 nanotubes as new visible-light-absorbing photocatalysts. *Appl. Phys. A* 127, 449. doi:10.1007/s00339-021-04574-x

Moon, G.-H., Fujitsuka, M., Kim, S., Majima, T., Wang, X., and Choi, W. (2017). Eco-friendly photochemical production of H_2O_2 through O_2 reduction over carbon nitride frameworks incorporated with multiple heteroelements. *ACS Catal.* 7, 2886–2895. doi:10.1021/acscatal.6b03334

Moon, G.-H., Kim, W., Bokare, A. D., Sung, N.-E., and Choi, W. (2014). Solar production of H_2O_2 on reduced graphene oxide–TiO_2 hybrid photocatalysts consisting of earth-abundant elements only. *Energy Environ. Sci.* 7, 4023–4028. doi:10.1039/c4ee02757d

Moreno, C. M. (2011). Hydrogen peroxide production driven by UV-B in planktonic microorganisms: A photocatalytic factor in sea warming and ice melting in regions with ozone depletion? *Biogeochemistry* 107, 1–8. doi:10.1007/s10533-010-9566-7

Noh, J. H., Yoo, S. H., Son, H., Fish, K. E., Douterelo, I., and Maeng, S. K. (2020). Effects of phosphate and hydrogen peroxide on the performance of a biological activated carbon filter for enhanced biofiltration. *J. Hazard Mater* 388, 121778. doi:10.1016/j.jhazmat.2019.121778

Peng, Y. L., Wang, L. Z., Liu, Y. D., Chen, H. J., Lei, J. Y., and Zhang, J. L. (2017). Visible-light-Driven photocatalytic H_2O_2 production on g-C_3N_4 loaded with CoP as a noble metal free cocatalyst. *Eur. J. Inorg. Chem.* 2017, 4797–4802. doi:10.1002/ejic.201700930

Qu, X., Hu, S., Bai, J., Li, P., Lu, G., and Kang, X. (2018). Synthesis of band gap-tunable alkali metal modified graphitic carbon nitride with outstanding photocatalytic H_2O_2 production ability via molten salt method. *J. Mater. Sci. Technol.* 34, 1932–1938. doi:10.1016/j.jmst.2018.04.019

Shiraishi, Y., Kanazawa, S., Kofuji, Y., Sakamoto, H., Ichikawa, S., Tanaka, S., et al. (2014a). Sunlight-driven hydrogen peroxide production from water and molecular oxygen by metal-free photocatalysts. *Angew. Chem. Int. Ed. Engl.* 53, 13454–13459. doi:10.1002/anie.201407938

Shiraishi, Y., Kanazawa, S., Sugano, Y., Tsukamoto, D., Sakamoto, H., Ichikawa, S., et al. (2014b). Highly selective production of hydrogen peroxide on graphitic carbon nitride (g-C_3N_4) photocatalyst activated by visible light. *Acs Catal.* 4, 774–780. doi:10.1021/cs401208c

Shiraishi, Y., Kanazawa, S., Tsukamoto, D., Shiro, A., Sugano, Y., and Hirai, T. (2013). Selective hydrogen peroxide formation by titanium dioxide photocatalysis with benzylic alcohols and molecular oxygen in water. *Acs Catal.* 3, 2222–2227. doi:10.1021/cs400511q

Shiraishi, Y., Takii, T., Hagi, T., Mori, S., Kofuji, Y., Kitagawa, Y., et al. (2019). Resorcinol-formaldehyde resins as metal-free semiconductor photocatalysts for solar-to-hydrogen peroxide energy conversion. *Nat. Mater* 18, 985–993. doi:10.1038/s41563-019-0398-0

Shu, C., Tan, Q., Deng, C., Du, W., Gan, Z., Liu, Y., et al. (2021). Hierarchically mesoporous carbon spheres coated with a single atomic Fe–N–C layer for balancing activity and mass transfer in fuel cells. *Carbon Energy* 4, 1–11. doi:10.1002/cey2.136

Song, H. Y., Wei, L. S., Chen, C. X., Wen, C. C., and Han, F. Q. (2019). Photocatalytic production of H_2O_2 and its *in situ* utilization over atomic-scale Au modified MoS_2 nanosheets. *J. Catal.* 376, 198–208. doi:10.1016/j.jcat.2019.06.015

Sterenchuk, T. P., Belykh, L. B., Skripov, N. I., Sanzhieva, S. B., Gvozdovskaya, K. L., and Schmidt, F. K. (2018). The effect of particle size and the modifier on the properties of palladium catalysts in the synthesis of hydrogen peroxide by the anthraquinone method. *Kinet. Catal.* 59, 585–592. doi:10.1134/S0023158418050166

Sun, Z., Sheng, L., Gong, H., Song, L., Jiang, X., Wang, S., et al. (2020). Electrocatalytic synthesis of hydrogen peroxide over Au/TiO_2 and electrochemical trace of OOH* intermediate. *Chem. Asian J.* 15, 4280–4285. doi:10.1002/asia.202001089

Teng, Z. Y., Cai, W., Liu, S. X., Wang, C. Y., Zhang, Q. T., Su, C. L., et al. (2020). Bandgap engineering of polymetric carbon nitride copolymerized by 2, 5, 8-triamino-tri-s-triazine (melem) and barbituric acid for efficient nonsacrificial photocatalytic H_2O_2 production. *Appl. Catal. B-Environmental* 271, 118917. doi:10.1016/j.apcatb.2020.118917

Teranishi, M., Kunimoto, T., Naya, S., Kobayashi, H., and Tada, H. (2020). Visible-light-Driven hydrogen peroxide synthesis by a hybrid photocatalyst consisting of bismuth vanadate and bis(hexafluoroacetylacetonato)copper(II) complex. *J. Phys. Chem. C* 124, 3715–3721. doi:10.1021/acs.jpcc.9b11568

Teranishi, M., Naya, S., and Tada, H. (2010). *In situ* liquid phase synthesis of hydrogen peroxide from molecular oxygen using gold nanoparticle-loaded titanium(IV) dioxide photocatalyst. *J. Am. Chem. Soc.* 132, 7850–7851. doi:10.1021/ja102651g

Teranishi, M., Naya, S., and Tada, H. (2016). Temperature- and pH-dependence of hydrogen peroxide formation from molecular oxygen by gold nanoparticle-loaded titanium(IV) oxide photocatalyst. *J. Phys. Chem. C* 120, 1083–1088. doi:10.1021/acs.jpcc.5b10626

Tian, J., Wu, T. J., Wang, D., Pei, Y., Qiao, M. H., and Zong, B. N. (2019). One-pot synthesis of potassium and phosphorus-doped carbon nitride catalyst derived from urea for highly efficient visible light-driven hydrogen peroxide production. *Catal. Today* 330, 171–178. doi:10.1016/j.cattod.2018.07.039

Tsukamoto, D., Shiro, A., Shiraishi, Y., Sugano, Y., Ichikawa, S., Tanaka, S., et al. (2012). Photocatalytic H2O2 production from ethanol/O2 system using TiO2 loaded with Au–Ag bimetallic alloy nanoparticles. *ACS Catal.* 2, 599–603. doi:10.1021/cs2006873

Viswanathan, V., Hansen, H. A., Rossmeisl, J., and Norskov, J. K. (2012). Unifying the 2e(-) and 4e(-) Reduction of Oxygen on Metal Surfaces. *J. Phys. Chem. Lett.* 3, 2948–2951. doi:10.1021/jz301476w

Wang, H., Guan, Y., Hu, S., Pei, Y., Ma, W., and Fan, Z. (2019b). Hydrothermal synthesis of band gap-tunable oxygen-doped g-C_3N_4 with outstanding "two-channel" photocatalytic H_2O_2 production ability assisted by dissolution–precipitation process. *Nano* 14, 1950023. doi:10.1142/s1793292019500231

Wang, L. C., Cao, S., Guo, K., Wu, Z. J., Ma, Z., and Piao, L. Y. (2019a). Simultaneous hydrogen and peroxide production by photocatalytic water splitting. *Chin. J. Catal.*, 40, 470–475. doi:10.1016/S1872-2067(19)63274-2

Wang, Y., Shi, L., Zhu, J., Li, B., and Jin, Y. (2020a). Visual and sensitive detection of telomerase activity via hydrogen peroxide test strip. *Biosens. Bioelectron.* 156, 112132. doi:10.1016/j.bios.2020.112132

Wang, Z., Huang, J., Mao, J., Guo, Q., Chen, Z., and Lai, Y. (2020b). Metal–organic frameworks and their derivatives with graphene composites: Preparation and applications in electrocatalysis and photocatalysis. *J. Mater. Chem. A* 8, 2934–2961. doi:10.1039/c9ta12776c

Wei, Z., Liu, M. L., Zhang, Z. J., Yao, W. Q., Tan, H. W., and Zhu, Y. F. (2018). Efficient visible-light-driven selective oxygen reduction to hydrogen peroxide by oxygen-enriched graphitic carbon nitride polymers. *Energy & Environ. Sci.* 11, 2581–2589. doi:10.1039/c8ee01316k

Willis, D. E., Taheri, M. M., Kizilkaya, O., Leite, T. R., Zhang, L., Ofoegbuna, T., et al. (2020). Critical coupling of visible light extends hot-electron lifetimes for H_2O_2 synthesis. *ACS Appl. Mater Interfaces* 12, 22778–22788. doi:10.1021/acsami.0c00825

Wu, G., Hu, S., Han, Z., Liu, C., and Li, Q. (2017). The effect of Ni(i)–N active sites on the photocatalytic H_2O_2 production ability over nickel doped graphitic carbon nitride nanofibers. *New J. Chem.* 41, 15289–15297. doi:10.1039/c7nj03298f

Xu, J., Chen, Z., Zhang, H., Lin, G., Lin, H., Wang, X., et al. (2017). $Cd_3(C_3N_3S_3)_2$ coordination polymer/graphene nanoarchitectures for enhanced photocatalytic H_2O_2 production under visible light. *Sci. Bull.* 62, 610–618. doi:10.1016/j.scib.2017.04.013

Yan, X., Jia, Y., Wang, K., Jin, Z., Dong, C. L., Huang, Y. C., et al. (2020). Controllable synthesis of Fe–N_4 species for acidic oxygen reduction. *Carbon Energy* 2, 452–460. doi:10.1002/cey2.47

Yang, H. (2021). A short review on heterojunction photocatalysts: Carrier transfer behavior and photocatalytic mechanisms. *Mater. Res. Bull.* 142, 111406. doi:10.1016/j.materresbull.2021.111406

Yang, L. P., Dong, G. H., Jacobs, D. L., Wang, Y. H., Zang, L., and Wang, C. Y. (2017). Two-channel photocatalytic production of H_2O_2 over g-C_3N_4 nanosheets modified with perylene imides. *J. Catal.* 352, 274–281. doi:10.1016/j.jcat.2017.05.010

Yang, S., Verdaguer-Casadevall, A., Arnarson, L., Silvio, L., Colic, V., Frydendal, R., et al. (2018). Toward the decentralized electrochemical production of H_2O_2: A focus on the catalysis. *Acs Catal.* 8, 4064–4081. doi:10.1021/acscatal.8b00217

Ye, Y. X., Wen, C., Pan, J. H., Wang, J. W., Tong, Y. J., Wei, S. B., et al. (2021). Visible-light driven efficient overall H_2O_2 production on modified graphitic carbon nitride under ambient conditions. *Appl. Catal. B-Environmental* 285, 119726. doi:10.1016/j.apcatb.2020.119726

Younis, S. A., Kwon, E. E., Qasim, M., Kim, K. H., Kim, T., Kukkar, D., et al. (2020). Metal-organic framework as a photocatalyst: Progress in modulation strategies and environmental/energy applications. *Prog. Energy Combust. Sci.* 81, 100870. doi:10.1016/j.pecs.2020.100870

Zeng, X. K., Liu, Y., Kang, Y., Li, Q. Y., Xia, Y., Zhu, Y. L., et al. (2020). Simultaneously tuning charge separation and oxygen reduction pathway on graphitic carbon nitride by polyethylenimine for boosted photocatalytic hydrogen peroxide production. *Acs Catal.* 10, 3697–3706. doi:10.1021/acscatal.9b05247

Zeng, X. K., Wang, Z. Y., Wang, G., Gengenbach, T. R., Mccarthy, D. T., Deletic, A., et al. (2017). Highly dispersed TiO_2 nanocrystals and WO_3 nanorods on reduced graphene oxide: Z-Scheme photocatalysis system for accelerated photocatalytic water disinfection. *Appl. Catal. B-Environmental* 218, 163–173. doi:10.1016/j.apcatb.2017.06.055

Zhang, C., Bai, J., Ma, L., Lv, Y., Wang, F., Zhang, X., et al. (2018). Synthesis of halogen doped graphite carbon nitride nanorods with outstanding photocatalytic H_2O_2 production ability via saturated NH_4X (X = Cl, Br) solution-hydrothermal post-treatment. *Diam. Relat. Mater.* 87, 215–222. doi:10.1016/j.diamond.2018.06.013

Zhang, J., Yang, H., Gao, J., Xi, S., Cai, W., Zhang, J., et al. (2020a). Design of hierarchical, three-dimensional free-standing single-atom electrode for H_2O_2 production in acidic media. *Carbon Energy* 2, 276–282. doi:10.1002/cey2.33

Zhang, M. M., Lai, C., Li, B. S., Xu, F. H., Huang, D. L., Liu, S. Y., et al. (2020b). Unravelling the role of dual quantum dots cocatalyst in 0D/2D heterojunction photocatalyst for promoting photocatalytic organic pollutant degradation. *Chem. Eng. J.* 396, 125343. doi:10.1016/j.cej.2020.125343

Zhang, W., Liu, Z., Chen, P., Zhou, G., Liu, Z., and Xu, Y. (2021). Preparation of supported perovskite catalyst to purify membrane concentrate of coal chemical wastewater in UV-catalytic wet hydrogen peroxide oxidation system. *Int. J. Environ. Res. Public Health* 18, 4906. doi:10.3390/ijerph18094906

Zhao, Z. H., Fan, J. M., Chang, H. H., Asakura, Y., and Yin, S. (2017). Recent progress on mixed-anion type visible-light induced photocatalysts. *Sci. China-Technological Sci.* 60, 1447–1457. doi:10.1007/s11431-016-9022-9

Zheng, L. H., Su, H. R., Zhang, J. Z., Walekar, L. S., Molamahmood, H. V., Zhou, B. X., et al. (2018). Highly selective photocatalytic production of H_2O_2 on sulfur and nitrogen for co-doped graphene quantum dots tuned TiO_2. *Appl. Catal. B-Environmental* 239, 475–484. doi:10.1016/j.apcatb.2018.08.031

Zinola, C. F., Triaca, W. E., and Arvia, A. J. (1995). Kinetics and mechanism of the oxygen electroreduction reaction on faceted platinum-electrodes in trifluoromethanesulfonic acid-solutions. *J. Appl. Electrochem.*, 25, 740–754. doi:10.1007/Bf00648629

Zuo, G. F., Li, B. D., Guo, Z. L., Wang, L., Yang, F., Hou, W. S., et al. (2019b). Efficient photocatalytic hydrogen peroxide production over TiO_2 passivated by SnO_2. *Catalysts* 9, 623. doi:10.3390/catal9070623

Zuo, G. F., Liu, S. S., Wang, L., Song, H., Zong, P. X., Hou, W. S., et al. (2019a). Finely dispersed Au nanoparticles on graphitic carbon nitride as highly active photocatalyst for hydrogen peroxide production. *Catal. Commun.* 123, 69–72. doi:10.1016/j.catcom.2019.02.011

Zuo, G., Zhang, Y., Liu, S., Guo, Z., Zhao, Q., Saianand, G., et al. (2020). A beta-cyclodextrin modified graphitic carbon nitride with Au Co-catalyst for efficient photocatalytic hydrogen peroxide production. *Nanomater. (Basel)* 10, 1969. doi:10.3390/nano10101969